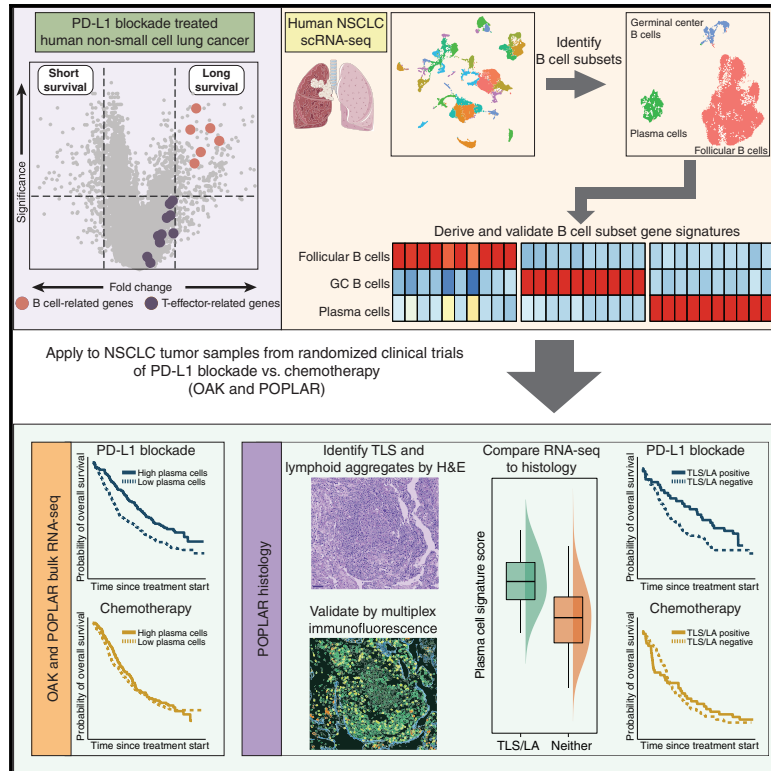


Intratumoral plasma cells predict outcomes to PD-L1 blockade in non-small cell lung cancer

Graphical abstract



Authors

Namrata S. Patil, Barzin Y. Nabet, Sören Müller, ..., Marcus Ballinger, Romain Banchereau, David S. Shames

Correspondence

patil.namrata@gene.com (N.S.P.), nabet.barzin@gene.com (B.Y.N.)

In brief

Patil et al. utilize scRNA-seq of NSCLC tumors to identify three main populations of intratumoral B and plasma cells. Deconvolution of bulk RNA-seq of two large randomized NSCLC clinical trials demonstrates a strong association of increased intratumoral plasma cells with longer overall survival in patients treated with PD-L1 blockade, but not with chemotherapy.

Highlights

- Three populations of intratumoral B and plasma cells identified by scRNA-seq in NSCLC
- Plasma cells show the strongest predictive association with OS to PD-L1 blockade
- Plasma cell benefits are independent of intratumoral CD8 T cells and PD-L1 expression
- B and plasma cells are present in tertiary lymphoid structures in NSCLC tumors

Article

Intratumoral plasma cells predict outcomes to PD-L1 blockade in non-small cell lung cancer

Namrata S. Patil,^{1,7,8,*} Barzin Y. Nabet,^{1,7,*} Sören Müller,² Hartmut Koeppen,³ Wei Zou,¹ Jennifer Giltneane,³ Amelia Au-Yeung,⁴ Shyam Srivats,¹ Jason H. Cheng,¹ Chikara Takahashi,⁴ Patricia E. de Almeida,⁵ Avantika S. Chitre,⁵ Jane L. Grogan,⁵ Linda Rangell,³ Sangeeta Jayakar,³ Maureen Peterson,¹ Allison W. Hsia,¹ William E. O’Gorman,⁴ Marcus Ballinger,⁶ Romain Banchereau,¹ and David S. Shames¹

¹Oncology Biomarker Development, Genentech, Inc., South San Francisco, CA, USA

²Oncology Bioinformatics, Genentech, Inc., South San Francisco, CA, USA

³Research Pathology, Genentech, Inc., South San Francisco, CA, USA

⁴OMNI Biomarker Development, Genentech, Inc., South San Francisco, CA, USA

⁵Cancer Immunology Research, Genentech, Inc., South San Francisco, CA, USA

⁶Clinical Science, Genentech, Inc., South San Francisco, CA, USA

⁷These authors contributed equally

⁸Lead contact

*Correspondence: patil.namrata@gene.com (N.S.P.), nabet.barzin@gene.com (B.Y.N.)

<https://doi.org/10.1016/j.ccell.2022.02.002>

SUMMARY

Inhibitors of the programmed cell death-1 (PD-1/PD-L1) signaling axis are approved to treat non-small cell lung cancer (NSCLC) patients, based on their significant overall survival (OS) benefit. Using transcriptomic analysis of 891 NSCLC tumors from patients treated with either the PD-L1 inhibitor atezolizumab or chemotherapy from two large randomized clinical trials, we find a significant B cell association with extended OS with PD-L1 blockade, independent of CD8⁺ T cell signals. We then derive gene signatures corresponding to the dominant B cell subsets present in NSCLC from single-cell RNA sequencing (RNA-seq) data. Importantly, we find increased plasma cell signatures to be predictive of OS in patients treated with atezolizumab, but not chemotherapy. B and plasma cells are also associated with the presence of tertiary lymphoid structures and organized lymphoid aggregates. Our results suggest an important contribution of B and plasma cells to the efficacy of PD-L1 blockade in NSCLC.

INTRODUCTION

Lung cancer is the leading cause of cancer-related death worldwide. Eighty to eighty-five percent of lung cancers are of the non-small cell lung cancer (NSCLC) subtype (Duma et al., 2019). Monoclonal antibodies against immune checkpoints, including programmed cell death-1 (PD-1) and its ligand PD-L1, have provided up to 40% response rate in the monotherapy setting (Mok et al., 2019). PD-(L)1 blockade in NSCLC is marked by durable efficacy that results in significant overall survival benefit (Grant et al., 2021). However, most NSCLC patients do not respond to PD-(L)1 blockade as single agents, and intratumoral immune infiltrates involved in the response to these therapies remain poorly characterized (Camidge et al., 2019).

Atezolizumab is a monoclonal antibody targeting PD-L1 that disrupts the PD-L1:PD-1 interaction and the PD-L1:B7-1 *cis* interaction (Zhao et al., 2019). In NSCLC, atezolizumab is approved in the United States for first line as monotherapy in patients with high PD-L1 expression on tumor cells and/or intratumoral immune cells (Herbst et al., 2020), as a second-line treatment in all cancer immunotherapy (CIT)-naïve patients (Rittmeyer et al., 2017) and as a first-line combination treatment with chemotherapy (paclitaxel and carboplatin) and the VEGF inhibitor bevacizumab (Reck et al., 2019; Socinski et al., 2018).

Greater benefit from atezolizumab is observed in tumors with high PD-L1 expression (Rittmeyer et al., 2017), high T-effector- and interferon-gamma-associated gene expression (Facchinetti et al., 2018), and high tumor mutation burden (TMB) (Gandara et al., 2018). However, there remains a significant need to understand the biology of response and resistance and the role of infiltrating immune cells. The association between CD8⁺ T cell infiltration and response to checkpoint inhibitors (CPIs) has been described across multiple indications (Waldman et al., 2020). Recent studies have also identified an association between increased B cell infiltration, along with the presence of tertiary lymphoid structures (TLSs) and improved response to immunotherapy in tumors from melanoma, soft tissue sarcoma, and renal cell carcinoma patients (Cabrita et al., 2020; Helmink et al., 2020; Petitprez et al., 2020). Importantly, these studies found patients exhibiting tumors with high expression of B cell gene signatures to show favorable prognosis in these indications based on single-arm studies and tumors from The Cancer Genome Atlas (TCGA), irrespective of treatment modality (Cabrita et al., 2020; Helmink et al., 2020; Petitprez et al., 2020). As such, it is unclear whether intratumoral B cells are beneficial specifically in the context of PD-(L)1 blockade or are a general marker of a better prognosis in metastatic NSCLC.

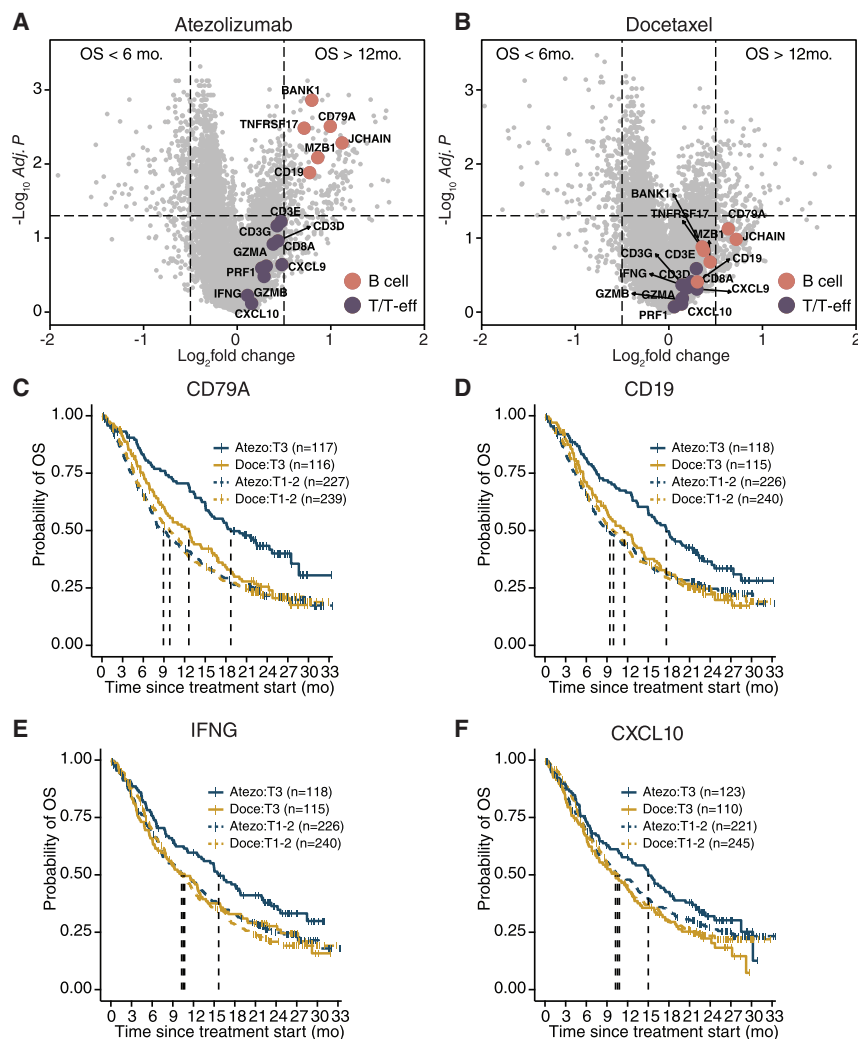


Figure 1. Intratumoral B cells associate with increased OS in NSCLC patients treated with atezolizumab

(A) Volcano plot depicting differentially expressed genes (FDR $p < 0.05$; absolute $\log_{2}FC \geq 0.5$) between patients from OAK with OS < 6 months ($n = 205$) versus OS > 12 months ($n = 205$) after treatment with atezolizumab. Hallmark B and plasma cell genes and T-effector genes are represented in orange and purple, respectively.

(B) Same as (A) in patients treated with docetaxel. (C–F) Kaplan Meier (KM) curves comparing the probability of survival in patients enriched for CD79A, CD19, IFNG, and the IFN-inducible chemokine CXCL10. Gene expression was dichotomized as high (top tertile T3) or low/intermediate (tertiles T1 and T2).

See also related [Figure S1](#) and [Tables S2](#) and [S3](#).

the presence of CD8⁺ T cells, in NSCLC patients who derive an OS benefit from PD-L1 checkpoint blockade.

RESULTS

A B cell transcriptional signature associates with prolonged OS in patients treated with atezolizumab

We first sought to identify differentially expressed genes (DE-Gs) between tumors from patients with or without OS benefit to atezolizumab in OAK, comparing patients with long survival (> 12 months; $n = 313$) and those with short survival (< 6 months; $n = 205$) within each treatment arm. Between patients with long or short OS with atezolizumab, 817 genes were differentially expressed (false discovery

rate [FDR]-corrected $p < 0.01$; absolute $\log_{2}FC \geq 0.5$; [Table S2](#)). The top over-expressed genes were enriched for genes associated with B and plasma cell biology, including *CD19*, *CD79A*, *BANK1*, *JCHAIN*, *MZB1*, and *TNFRSF17* (B cell maturation antigen [BCMA]; [Figure 1A](#)). Genes associated with cytotoxic T cell and interferon (IFN) signals (*CD3E*, *D*, *G*, *CD8A*, *GZMA-B*, *IFNG*, and *CXCL9-10*) were also detected, albeit not significantly. None of these genes were significant in the docetaxel arm ([Figure 1B](#); [Table S3](#)), suggesting a predictive value of these B and plasma cell genes specifically for response to atezolizumab. These observations were validated in the phase II randomized clinical trial POPLAR ([Figures S1A](#) and [S1B](#)).

We then validated results from linear modeling by deriving Kaplan-Meier curves in OAK, categorizing gene expression by tertiles, and comparing high expression (T3) versus low/intermediate (T1-T2) combined. High expression of the B cell markers *CD79A* (hazard ratio [HR] atezolizumab: 0.54 [0.41–0.72]; HR chemo: 0.88 [0.67–1.13]) and *CD19* (HR atezolizumab: 0.65 [0.50–0.86]; HR chemo: 0.94 [0.72–1.2]) provided increased OS benefit over *IFNG* (HR atezolizumab: 0.73 [0.55–0.96]; HR chemo: 0.95 [0.73–1.23]) or the IFN-inducible chemokine

Herein, we analyzed the transcriptomes of 891 pre-treatment tumors from POPLAR (phase 2; [Fehrenbacher et al., 2016](#)) and OAK (phase 3; [Rittmeyer et al., 2017](#)), two randomized clinical trials of atezolizumab versus chemotherapy (docetaxel) in NSCLC, representing the largest transcriptional collection assembled to date in NSCLC in these settings ([Table S1](#)). We first identified a robust B and plasma cell signal associated with overall survival (OS) benefit in patients treated with atezolizumab, but not docetaxel, in both trials. We then leveraged a large single-cell RNA sequencing (scRNA-seq) NSCLC dataset to identify specific transcriptional signatures for intratumoral follicular B cells, germinal center B cells, and plasma cells, which were validated at the protein level by cytometry by time of flight (CyTOF). Deconvolution of these signatures in our large transcriptional datasets highlighted the importance of plasma cells toward OS benefit with atezolizumab, independently of CD8⁺ T cell signatures. Finally, intratumoral enrichment of the plasma cell signature associated with the presence of TLSs and/or lymphoid aggregates, supporting a specific spatial organization for B and plasma cell activity within tumors. Our study reveals the importance of intratumoral B and plasma cells, independent of

CXCL10 (HR atezolizumab: 0.85 [0.65–1.11]; HR chemo: 1.11 [0.85–1.44]; **Figures 1C–1F**). Again, similar results were observed for POPLAR (**Figures S1C–S1F**).

To confirm these transcriptional findings at the protein level, we evaluated baseline tumor samples from two responders and two non-responders to atezolizumab by immunofluorescence (IF) staining for CD8, CD79, and Ki67 using multiplex IF. Abundant CD79⁺ B cells were detected in tumors from patients with objective responses compared with those without (**Figure S1G**). In addition, multiplex immunohistochemistry (IHC) detected regions where CD8⁺ T cells were in close proximity ($9.9 \pm 1.69 \mu\text{m}$ apart) with CD79⁺ B cells, suggestive of B cell-T cell interactions (**Cabrita et al., 2020**).

Identification of B cell subsets by single-cell RNA-seq

To further characterize the B cell compartment involved in response to atezolizumab, we analyzed a large scRNA-seq dataset of 208,506 cells collected from lung and peripheral tissue from 44 NSCLC patients (**Kim et al., 2020**), focusing on the B and plasma cell populations. Aggregating cells from tumor and draining lymph node compartments, dimensionality reduction with uniform manifold approximation and projection (UMAP), and graph-based clustering identified three major CD79A⁺ B cell subsets across tumors, including follicular B cells, germinal center (GC) B cells, and plasma cells (**Figure 2A**). While we found an increased number of B and plasma cells in tumor tissue compared with normal adjacent tissue (NAT), the composition of GC, follicular B, and plasma cells within these B cell populations was similar between tumor and NAT from the same patient (**Figure 2B**). Transcriptional signatures specific to each subset were identified. Follicular B cells were enriched for *CD83*, *CD69*, *SELL*, and *BANK1* (**Aiba et al., 2006**). Plasma cells were enriched for several immunoglobulin transcripts (*IGHG2*, *IGHG1*, and *IGHA2*), *MZB1*, *DERL3*, and *XBP1* (**Shaffer et al., 2004**). GC center B cells were enriched for *HMG1*, *AICDA*, and *RGS13* (**Ruffin et al., 2021**). We refined these signatures by probing the expression of these transcripts across multiple immune (myeloid, NK, and T cells), stromal (fibroblasts and endothelial cells), and epithelial and tumor cell populations (**Figure S2A**) from the same patients, only retaining genes specific for B cell compartments. We further focused only on markers with a high degree of specificity for the individual B cell populations (**Figures 2C and S2A**).

We validated the three scRNA-seq-derived signatures (follicular and GC B and plasma cells) in two independent NSCLC scRNA-seq datasets (**Lambrechts et al., 2018**; **Maynard et al., 2020**). We found two distinct clusters of B cells in the data from Lambrechts et al. (**Figure S2B**, top), and expression of individual genes as well as scoring cells for our previously derived gene signatures clearly identified one of them as follicular B cells and the other one as plasma cells (**Figure S2B**, bottom). No cluster of GC B cells was found in the Lambrechts et al. dataset, reflecting the limited cohort size and overall low prevalence of TLSs. Analysis of the NSCLC scRNA-seq from Maynard et al. revealed three clusters of B and plasma cells, which we identified as follicular B cells, plasma cells, or GC B cells using individual genes as well as enrichment analysis of our gene signatures (**Figures 2D and 2E**).

We complemented this transcriptional approach with mass cytometry, using a 38-marker CyTOF panel on single-cell suspensions from six procured NSCLC tumors (**Banchereau et al.,**

2021a). Our analysis confirmed the presence of three intratumoral B cell populations, based on CD19, human leukocyte antigen – DR subtype (HLA-DR), CD38, and Ki67 staining (plasma cells: CD38⁺, HLA-DR⁺, Ki67⁺; GC B cells: CD38⁺, HLA-DR⁺, Ki67⁺; follicular B cells: CD38⁺, HLA-DR⁺, Ki67⁺; **Figure S2C**). These markers showed similar expression patterns in the scRNA-seq dataset (**Figure S2D**). In summary, we identified expression signatures consistently identifying follicular B cells, plasma cells, and GC B cells across three independent NSCLC scRNA-seq datasets. The presence of these three populations was further confirmed at the protein level using CyTOF.

scRNA-seq-derived signatures for bulk RNA-seq analysis

We then asked whether these B cell signatures identified from scRNA-seq analyses could predict patient survival following treatment with atezolizumab or docetaxel. We first validated that signatures derived from scRNA-seq could be applied to bulk RNA-seq data by measuring gene co-expression and performing hierarchical clustering on these co-expression patterns (**Figures 3A and S3A**). Our analyses revealed high correlation between expression of GC and follicular B cells markers in bulk tumors (**Figure S3B**; $R = 0.74$). Plasma cell markers were also strongly correlated but showed lower correlations with GC or follicular B cell markers (**Figure S3B**; mean $R = 0.5$). Importantly, we found no correlation between plasma cell signature scores and percent neoplastic cells defined by hematoxylin and eosin (H&E) stain ($R = -0.084$), suggesting that tumor purity is not a relevant confounder of these transcriptomic signatures (**Figure S3C**).

To additionally validate our signatures, we performed paired bulk RNA-seq and multiplex IF (mIF) on 23 NSCLC tumors. In a blinded review, a trained pathologist confirmed that CD138⁺/panCK⁺ cells in the non-tumor area matched plasma cells identified by H&E (**Figure 3B**). As expected, CD138 was only specific for plasma cells in the non-tumor area, whereas, in the tumor area, there were often panCK⁺/CD138⁺ cells that were negative for additional plasma cell markers (BCMA) and did not show plasma cell morphology (**Figure S5A**). The relationship between RNA-seq and mIF was then assessed by normalizing the mIF plasma cell quantification to total tumor panCK⁺ cells to account for differences in tumor size, since the RNA-seq data were derived from different serial sections of the same tissue blocks. Overall, quantification of plasma cells by mIF or RNA-seq was highly correlated (Spearman $R = 0.49$; $p = 0.02$; **Figure 3C**). Importantly, dichotomizing samples by the highest tertile (T3) versus the bottom two tertiles (T1-T2) yielded highly similar stratifications (**Figure 3D**). Moreover, the plasma cell RNA-seq signature genes individually correlated with the mIF plasma cell quantification, whereas the follicular B cell and GC signatures did not, highlighting the specificity of the plasma cell signature (**Figure 3E**). In sum, using an orthogonal method to quantify plasma cell infiltrate, we demonstrate that the scRNA-seq-derived signature (**Table S4**) is highly specific for plasma cells and adequate for further sample stratification by bulk RNA-seq.

High plasma cell signature predicts OS benefit from atezolizumab

We then dichotomized these signatures using the tertile split and comparing high (T3) versus low/intermediate (T1/T2) expression

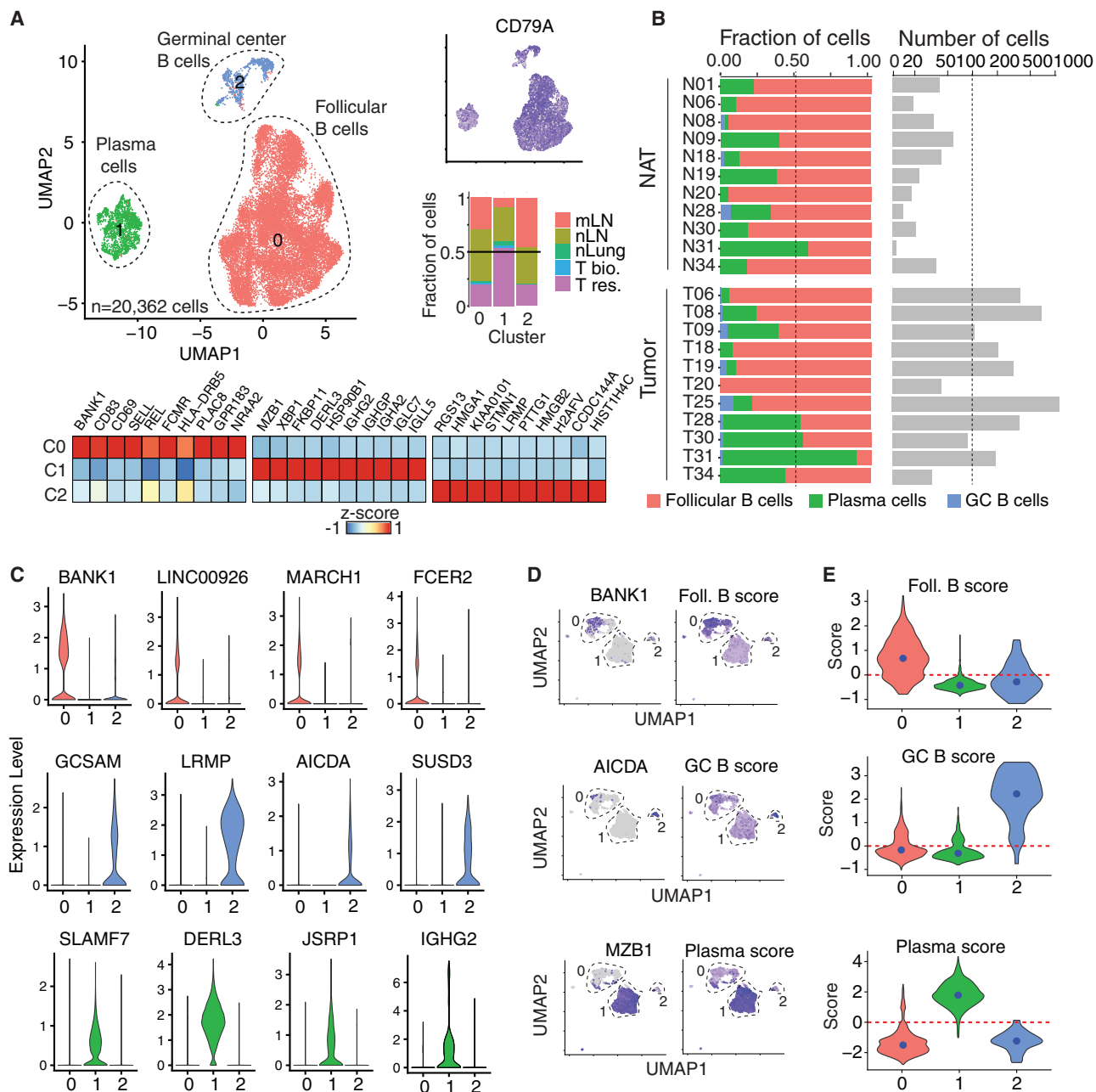


Figure 2. Identification of three B cell subsets in NSCLC tumors

(A) (Left) UMAP dimensionality reduction of 20,362 cells (dots) colored by cluster assignment. The same UMAP is given on the top right, here colored by *CD79A* expression. (Middle right) The fraction of cells in each cluster from metastatic lymph node (mLN), non-metastatic lymph node (nLN), normal adjacent lung tissue (nLung), tumor biopsy (T bio.), and tumor resection (T res) is shown. (Bottom) Relative average expression of indicated markers in clusters from (A) is shown.

(B) (Left) The fraction of cells comparing normal and tumor samples from each patient (rows) for clusters given in (A). (Right) Absolute numbers of cells from each patient for clusters in (A) are shown.

(C) Violin plots indicating the expression of marker genes in clusters from (A).

(A)–(C) are all based on the dataset from Kim et al. (2020).

(D) UMAPs of B cell clusters (Maynard et al., 2020) colored by expression of single marker genes (left) or scores for gene signatures derived for follicular B cells (top), GC B cells (middle), and plasma cells (bottom).

(E) Distribution of scores (y axis) across clusters (x axis) for signatures as shown in (D).

See also related Figure S2.

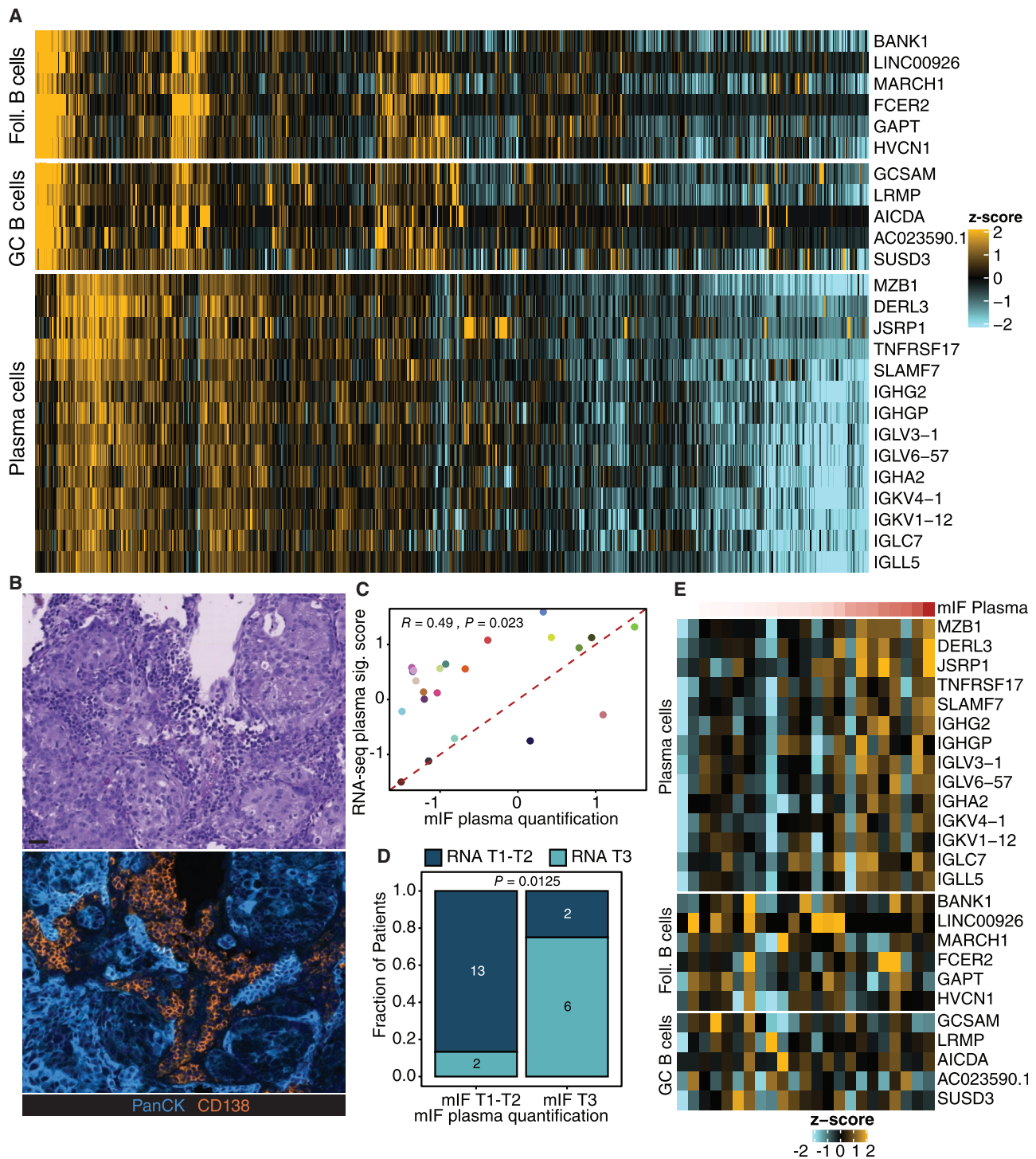


Figure 3. B cell subset signatures in bulk RNA-seq profiles

- (A) Hierarchical clustering of the three B cell signatures identified from the scRNA-seq data in OAK.
 (B) Representative NSCLC H&E (top) and mIF (bottom) demonstrating histologically defined plasma cells can be identified as CD138⁺/panCK⁻ cells. Scale bar indicates 50 μ m.
 (C) Correlation of mIF versus RNA-seq quantified plasma cells. The Spearman R value is reported.
 (D) Dichotomized plasma cell signature score and mIF quantified plasma cells by tertile. p value is a Fisher's exact test.
 (E) Expression of the genes that comprise the three B cell signatures ordered by increasing mIF plasma cell quantification.
 See also related [Figure S3](#) and [Table S4](#).

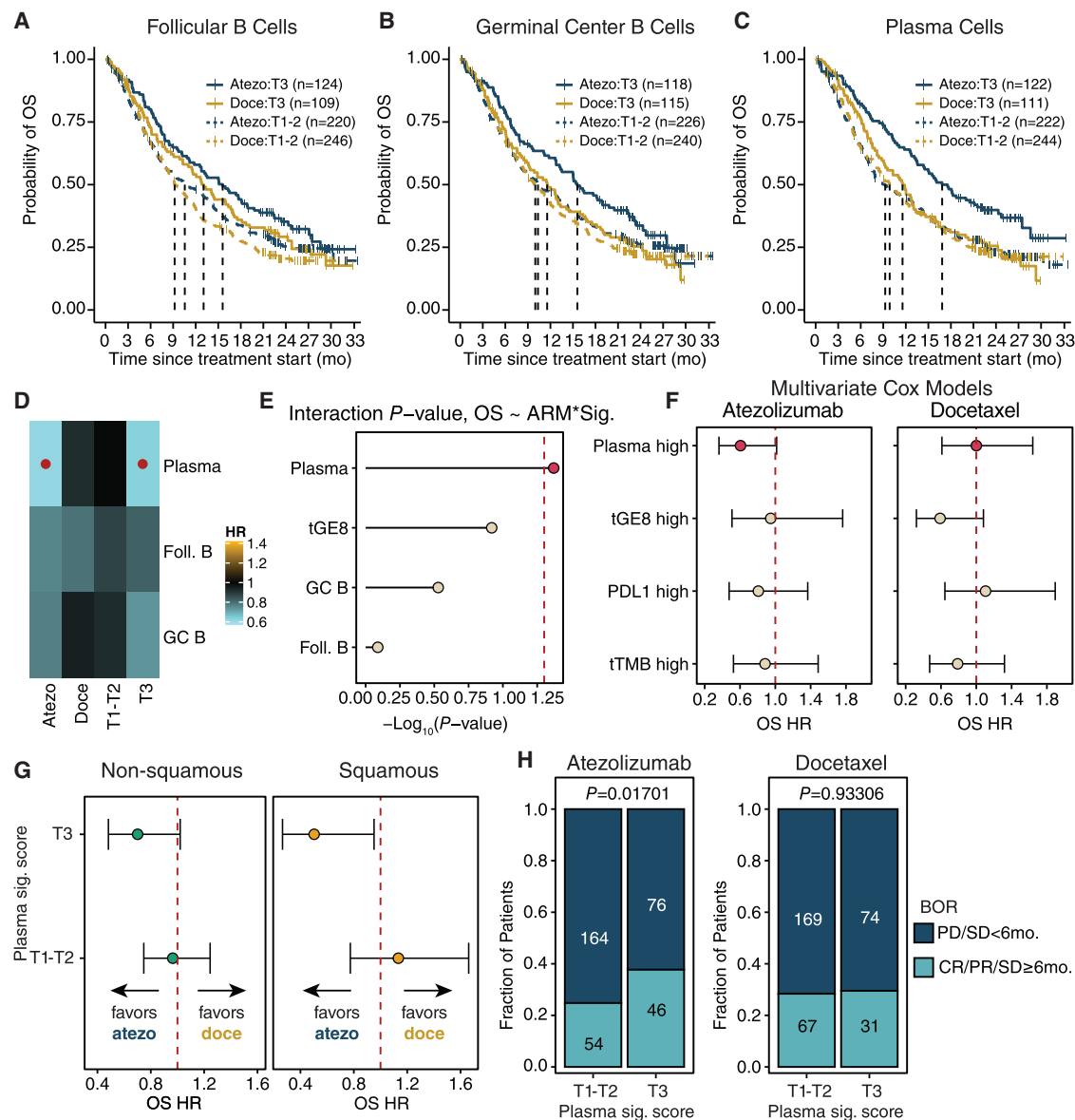


Figure 4. The plasma cell signature independently predicts response to atezolizumab

(A–C) Kaplan-Meier curves of OS for each of the indicated signatures, dichotomized as T3 (top tertile) versus T1-T2 (low/median tertiles).

(D) Heatmap depicting the results from Cox proportional hazard models testing hazard ratios within and across arms. Red dots represent statistically significant HRs ($p < 0.05$).

(E) Significance of the three B cell signatures and a previously reported 8-gene T-effector signature (tGE8) in univariate interaction models, where the interaction between signature score and treatment arm is considered.

(F) Forest plots depicting the significance of the plasma cell and tGE8 signatures with PD-L1 IHC (22C3 assay) and tissue TMB (FMI tTMB). Signatures are dichotomized as T3 versus T1-T2 in all models, tTMB utilizes a cut of 16, and PD-L1 $\geq 50\%$ tumor proportion score.

(G) Forest plots depicting atezolizumab versus docetaxel OS HRs separately by histology in the indicated plasma cell infiltration expression groups. Error bars represent 95% confidence intervals.

(H) Dichotomized plasma cell signature score by tertile stratifying best overall responses as objective responses or durable stable disease (SD) (with progression-free survival [PFS] ≥ 6 months) versus progressive disease or non-durable SD (with PFS < 6 months) within each arm. p value is a Fisher's exact test.

See also related [Figure S4](#).

groups. Kaplan-Meier analysis revealed that, while a trend toward OS benefit was observed with atezolizumab for the three signatures, only the plasma cell signature was significant (interaction $p < 0.05$) (atezolizumab high versus low HR = 0.63 [0.48–0.83]; chemo high versus low HR = 0.92 [0.71–1.2]; atezo-

lizumab high versus chemo high HR = 0.64 [0.47–0.88]; [Figures 4A–4D](#)). There was a similar strong stratification of OS by the plasma cell signature in POPLAR ([Figures S4A–S4C](#)). The potential predictive value of the plasma cell signature was confirmed in models testing the interaction of each signature with treatment

arms (Figure 4E). Importantly, neither the GC B cell, follicular B cell, nor our 8-gene T-effector signature tGE8 (composed of *IFNG*, *CXCL9*, *CD8A*, *GZMA*, *GZMB*, *CXCL10*, *PRF1*, and *TBX21*; Mariathasan et al., 2018) were significant in these models (Figure 4E). The predictive value of the plasma cell signature also held in multivariate models, including all four signatures (atezolizumab HR = 0.67 [0.50–0.89]; chemo HR = 0.94 [0.70–1.26]), confirming that the effect observed with the plasma cell signature may be specific and independent of CD8 T cell presence (Figure S4D).

Within our cohort, 207 patients (atezolizumab n = 99; docetaxel n = 108) had comprehensive biomarker profiling with PD-L1 IHC (22C3 assay), RNA-seq, and tissue TMB (FMI tTMB). To assess the predictive value and independence of the plasma cell signatures compared with known biomarkers of CPI response, we combined these features in a multivariate Cox proportional hazard analysis (plasma cell signature high, tGE8 signature high, PD-L1 $\geq 50\%$, and tTMB ≥ 16). Here, we find that the plasma cell signature has the strongest effect on OS in the atezo arm (plasma HR: 0.61 [0.36–1.01]). These associations were absent in the docetaxel arm (plasma HR: 1.00 [0.61–1.64]), underscoring the specificity of these signals with benefit, but not chemotherapy (Figure 4F).

In other indications, the increased presence of intratumoral B cells has potential prognostic implications in TCGA (Cabrita et al., 2020; Helmink et al., 2020; Petitprez et al., 2020); however, our data suggest a predictive signal for plasma-cell-rich NSCLC tumors specifically with immune checkpoint inhibition. Indeed, the plasma cell signature dichotomized by tertile split in TCGA NSCLC tumors had no impact on stratification of overall survival (Figure S4E). We further tested the plasma cell signature in our previously published study in urothelial cancer (IMvigor210, single arm of atezolizumab; Mariathasan et al., 2018). The signature was dichotomized as high versus low around the median expression. Patients with high plasma cell signature expression exhibited longer OS (HR = 0.77; p = 0.05; Figure S4F). In IMvigor210, we also observed a significant and positive association with OS in IMvigor210 and the continuous plasma cell signature score (HR = 0.84; p = 0.02), suggesting that this phenomenon may not be restricted to only NSCLC. In total, these data suggest that plasma-cell-rich tumors may portend OS benefit in patients treated with immune CPIs.

While OS is the gold standard for assessing CPI benefit in NSCLC, we also explored whether these findings are replicated when considering objective responses defined by RECIST 1.1 (Eisenhauer et al., 2009). Indeed, plasma cell high tumors showed significantly more patients who experienced clinical benefit, defined as best overall response of complete response, partial response, or durable stable disease (SD) (≥ 6 months), only in the atezolizumab arm (Figure 4H). Gene set enrichment analyses demonstrated enrichment of the plasma cell signature in patients with clinical benefit compared with those without clinical benefit in the atezolizumab arm (Figure S4G), but not in the docetaxel arm (Figure S4H). These data further underscore the importance of the plasma cell signature for predicting clinical benefit specifically to atezolizumab with different outcome parameters.

In addition, the strength of the plasma cell signature for predicting atezolizumab benefit was sustained in several subgroup

analyses. When separating squamous and non-squamous NSCLC patients in OAK, patients in the top tertile of plasma cell signatures score in either histology demonstrated longer OS benefit of atezolizumab over docetaxel (Figure 4G). There were no significant differences in the bottom two tertiles between atezolizumab and docetaxel OS benefit (Figure 4G). Several mutations in NSCLC have been reported to be associated with either poor prognosis or specifically poor outcomes on CPI (Lisberg et al., 2018; Skoulidis et al., 2018; Wohlhieter et al., 2020). Though numbers are low, patients with high plasma cell signatures and mutations in EGFR, STK11, or KEAP1 maintain the trend of longer OS for atezolizumab compared with docetaxel in these subsets of patients (Figure S4I). These data underscore the applicability of the plasma cell signature for predicting outcomes to atezolizumab across patient subgroups.

The plasma cell signature is enriched in tumors with tertiary lymphoid structures and/or lymphoid aggregates

In previous studies, intratumoral B cells have been found in organized TLSs (Sharonov et al., 2020). We therefore evaluated baseline tumor H&E slides for the presence of TLS or lymphoid aggregates (LAs) only (no observed GCs) in the same samples we had performed RNA-seq and mIF to compare features of TLSs and LAs at the cellular phenotype level. We found that TLSs defined by H&E are marked by a distinct GC dominated by CD20⁺ B cells. The GC was surrounded by a mix of CD20⁺ B cells and CD3⁺ T cells, which were composed of both CD8⁻ (CD4⁺ T cells) and CD8⁺ T cells (Figures 5A and S5B). Moreover, all identified TLSs were marked by surrounding plasma cells in close proximity (Figures 5A and S5B). LAs had more mixed features with no distinct CD20⁺ GC, and the balance shifted in favor of CD3⁺ T cells over CD20⁺ B cells (Figure 5A). Plasma cells were also found in or around LAs (Figure 5A).

To further understand the relationship between plasma cells and other cell types, we explored correlations with other cell types via mIF. Here, we utilized a leave-one-out approach to assess the correlation between plasma cells and other cell types captured by mIF. Plasma cells were most correlated with T cell infiltrate (CD3⁺). Plasma cells' levels were equally correlated with tumor-associated macrophages (CD68⁺ or CD163⁺), CD8 T cells (CD3⁺/CD8⁺), and CD4 T cells (CD3⁺/CD8⁻), while also strongly correlated with overall B cells (CD20⁺; Figure S5C). Together, these data suggest that plasma cell infiltration may be linked to T cell infiltration in a TLS or LA. Indeed, plasma cells by mIF are enriched in samples containing TLS or LA (Figure S5D).

We therefore evaluated tumor H&E for the presence of TLSs or LAs in POPLAR. Of the 254 patient samples analyzed, 9% had TLS-like structures with GCs, 21% had LAs with no observed GCs, and the remaining 70% had no detectable TLSs or LAs. Lymph node metastases samples (4% of all samples) were excluded from this analysis. There was no difference (p = 0.47) in TLS or LA distribution between samples from atezolizumab or docetaxel treatment arms (Figure 5B). Patients with tumors containing TLSs and/or LAs exhibited significantly increased OS when treated with atezolizumab (HR = 0.60 [0.38–0.94]), but not with docetaxel (HR = 0.93 [0.62–1.41]; Figure 5C). Similar to the plasma cell signatures, these data suggest that

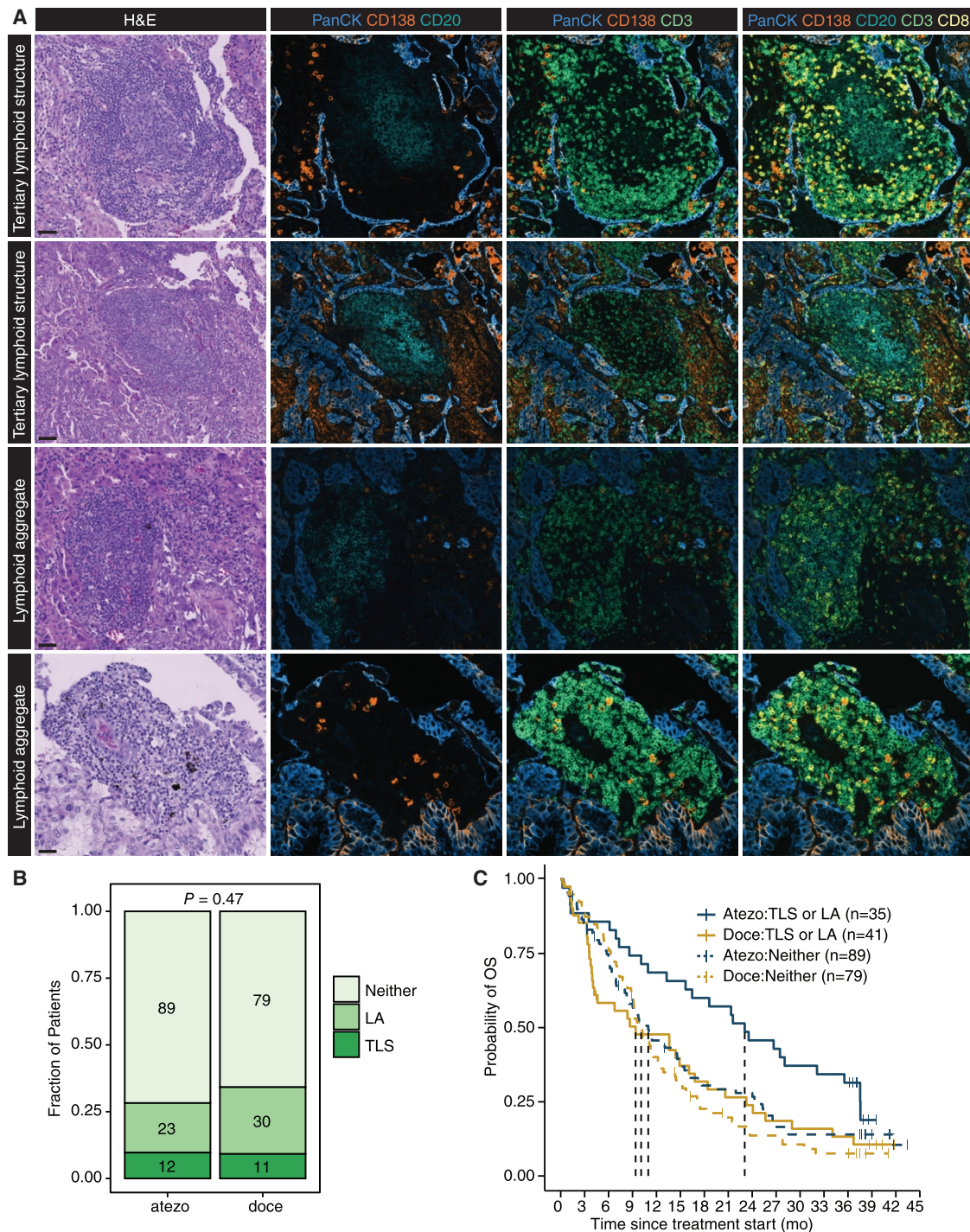


Figure 5. Patients with TLS/LA⁺ tumors exhibit improved OS with atezolizumab

(A) H&E staining and mIF for the indicated markers for representative TLSs (top two rows) and LAs (bottom two rows). Cellular phenotypes displayed are panCK⁺ (tumor cells), CD138⁺/panCK⁻ (plasma cells), CD3⁺ (T cells), CD20⁺ (B cells), CD3⁺/CD8⁺ (CD8 T cells), and CD3⁺/CD8⁻ (CD4 T cells). Scale bar indicates 50 μ m.

(B) Bar chart representing the proportion of tumors with TLSs, lymphoid aggregates (LAs) only, or neither in each treatment arm in POPLAR.

(C) Kaplan-Meier curve representing OS for tumors from POPLAR with TLSs or LAs identified by H&E versus those with neither, by treatment arm.

See also related [Figure S5](#).

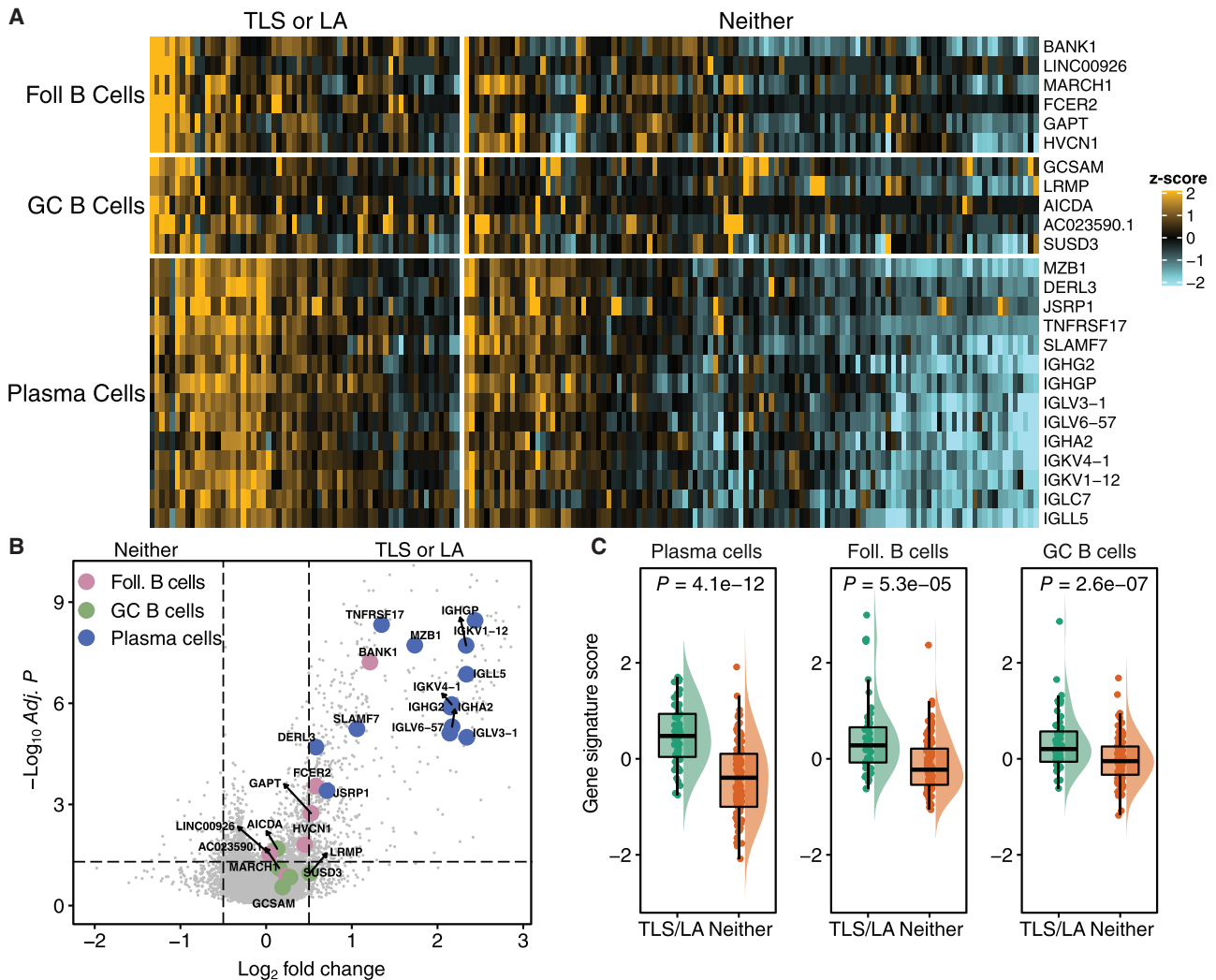


Figure 6. TLS/LA⁺ tumors are enriched for plasma cells

(A) Hierarchical cluster of the three B cell subset signatures. Samples are ordered by TLS and/or LA status in POPLAR.

(B) Volcano plot representing differentially expressed genes between tumors with TLS and/or LA versus tumors with neither in POPLAR. Genes from the three B cell signatures are highlighted.

(C) Violin plots depicting signature Z scores for the plasma cell, germinal center B cell, and follicular B cells, grouped by TLS and/or LA status in POPLAR. Wilcoxon p values are reported.

See also related [Figure S6](#).

TLS/LA presence is strongly associated with OS benefit specifically in atezolizumab-treated, but not docetaxel-treated, patients.

A linear model was then applied to identify DE-Gs between TLS/LA⁺ and TLS/LA⁻ tumors. Between the two groups, 928 genes were differentially expressed (FDR-corrected $p < 0.01$; absolute $\log_{2} \text{FC} \geq 0.5$). TLS/LA⁺ tumors were highly enriched for genes from each of the three intratumoral B cell subsets but especially plasma cell genes, including *MZB1*, *TNFRSF17* (BCMA), and immunoglobulins (Figures 6A and 6B). Quantitative analysis of the three B cell signatures confirmed the increase in plasma cells in TLS/LA⁺ tumors ($p = 4.1 \times 10^{-12}$). GC B cell ($p = 2.6 \times 10^{-7}$) and follicular B cell signatures ($p = 5.3 \times 10^{-5}$) were also increased in TLS/LA⁺ tumors (Figure 6C). Similarly, in the samples with paired mIF and RNA-seq, we found similar

enrichment of the plasma cell signature and related genes in samples with mIF-identified TLSs or LAs (Figures S6A and S6B).

Overall, our study integrating bulk transcriptomes from two large randomized clinical trials of atezolizumab versus docetaxel, as well as scRNA and protein measurement, demonstrated that the presence of high levels of intratumoral plasma cells in NSCLC associates strongly with longer OS in patients receiving atezolizumab.

DISCUSSION

Our data show that the presence of intratumoral B cells, especially plasma cells, at baseline is a key factor in determining the duration of OS in NSCLC patients treated with atezolizumab. Several studies have suggested that the presence of B cells

may be prognostic in several types of cancer (Blenman et al., 2018; Greiff et al., 2015; Knief et al., 2016; Nelson, 2010; Wouters and Nelson, 2018). Prior studies exploring B and plasma cells in NSCLC (Al-Shibli et al., 2008; Fujimoto et al., 2013; Gentles et al., 2015; Lohr et al., 2013) or TLS (Germain et al., 2014) have found that they are associated with better outcomes. These studies were almost exclusively conducted with early-stage settings, different treatment regimens, and in retrospective analyses across a mix of real-world and clinical trial samples. Therefore, the role of B cells in NSCLC in the context of immunotherapy in randomized trials has not been established (Patel et al., 2020). To our knowledge, our data provide the first substantial evidence that the presence of plasma cells and existence of organized lymphoid structures, such as TLSs at baseline, are associated with atezolizumab, but not with chemotherapy-mediated OS benefit. These data suggest a potential predictive rather than prognostic effect of these signals. To do so, we analyzed transcriptomic data from two large independent randomized clinical trial cohorts (OAK, $n = 699$ and POPLAR, $n = 192$), comprising the largest publicly available transcriptomic NSCLC database of patients treated with CPI or chemotherapy and their associated clinical outcome.

In our study, gene expression analyses revealed a strong association between B cell markers and longer OS with atezolizumab treatment. We utilized single cell analyses to derive and validate specific and robust gene signatures to reliably deconvolve follicular B cells, GC B cells, and plasma cells from bulk tumor transcriptomes. Importantly, these associations were found in subgroup analyses of histology and mutational status. While each B cell subset had some association with outcomes, plasma cells seem to be the most important. This is perhaps indicative of a productive local GC reaction whereby mature plasma cells are the end product. These data are bolstered by similarly significant clinical benefit in patients with histologically identified TLS or TLS-like structures. Moreover, using mIF, we find that TLSs are generally surrounded by plasma cells. Taken together, these data suggest that tumors with high plasma cell infiltration identify tumors with TLS or TLS-like structures that can provide sustained tumor killing once stimulated by CPI.

In our study, we confirmed TLS/LA identification by H&E with mIF in procured samples and then applied this approach to POPLAR. Here, tumors with TLS or LA comprised $\sim 30\%$ of all NSCLC tumors analyzed and were enriched for B and plasma cell signatures. The presence of TLS/LA is associated significantly with improved OS following treatment with atezolizumab, suggesting they may play an important role in sustained intratumoral immune responses with PD-(L)1 blockade. Supporting our findings, B-cell-rich TLSs have been associated with favorable outcomes in the context of immune checkpoint blockade for melanoma, soft tissue sarcoma, and renal cell carcinoma (RCC) (Cabrita et al., 2020; Helmink et al., 2020; Petitprez et al., 2020). These prior studies were limited by small cohorts of CPI-treated patients or with TCGA analyses and therefore only demonstrated largely prognostic associations with B and plasma cells and outcomes. When we applied the plasma cell signature to TCGA NSCLC transcriptomes from patients who were not primarily treated with CPI, we found no association with OS, suggesting that infiltration of plasma cells is not simply prognostic in NSCLC. Overall, our data in the context of two large randomized clinical

trials of atezolizumab versus chemotherapy show a strong predictive association between B and plasma cells and OS that is specific to PD-L1 blockade.

The mechanisms by which B and plasma cells contribute to anti-tumoral immunity remain unclear. Plasma cells may produce tumor-antigen-specific antibodies, leading to antibody-dependent cellular cytotoxicity and complement activation (Sharonov et al., 2020). B cells may also provide costimulatory signals to antigen-presenting cells (APCs) and $CD4^+$ T cells for an optimal response after countering inhibitory signals on exhausted cytotoxic T cells with PD-(L)1 blockade. While dendritic cells (DCs) are the main APCs, they migrate to secondary lymphoid organs once they are activated. On the other hand, mature B cells and plasma cells remain in the tumor and can form TLSs. B cells expressing specific B cell receptors (BCRs) can also act as an APC, capable of presenting antigen to $CD4^+$ and $CD8^+$ T cells (Adler et al., 2017; Bruno et al., 2017). These cells may be able to provide sustained co-stimulation to tumor-resident T lymphocytes and enable chemokine-mediated T lymphocyte tumor trafficking, thus contributing to the maintenance and expansion of long-term tumor immunity (Ruffin et al., 2021). Our analysis shows $CD79^+$ B cells and $CD8^+$ T cells are present in close proximity when visualized by IF imaging, supporting a role of these cells as APCs. Moreover, mIF demonstrated that plasma cells are highly correlated with CD4 and CD8 T cells, supporting a potential direct interaction. Class-switched and memory B cells were enriched in tumors from CIT responders in melanoma and RCC, where they may promote antigen presentation to prime cytotoxic T cells (Helmink et al., 2020; Petitprez et al., 2020). In support of the antigen presentation hypothesis, Bruno et al. (2017) have described that TIL-B cells influence the phenotype and function of $CD4^+$ TILs in NSCLC patient tumors *in vitro*.

Our analysis shows a significant correlation between TLSs defined by histology and B cell subset gene signatures, which clearly points to a common underlying B cell biology likely including a humoral immune response that contributes to the overall response to atezolizumab. The distinct B and plasma cell subtypes are intimately related. It is likely that the presence of intratumoral B and plasma cells relies on the development of mature TLSs. Our findings also clearly show that increased frequency of B and plasma cells at baseline associates with improved clinical outcome in NSCLC patients treated with atezolizumab, independently of cytotoxic T cell signatures. Novel therapeutics or combination therapies that engage both the cellular and humoral arms of the adaptive immune system may establish efficient immune surveillance mechanisms that will lead not only to tumor shrinkage and short-term responses but also can serve to reset the immune contexture of the tumor microenvironment, leading to sustained immune responses and OS benefit.

STAR★METHODS

Detailed methods are provided in the online version of this paper and include the following:

- KEY RESOURCES TABLE
- RESOURCE AVAILABILITY
 - Lead contact
 - Materials availability

- Data and code availability
- **EXPERIMENTAL MODEL AND SUBJECT DETAILS**
 - Patient population and biomarker collection
- **METHOD DETAILS**
 - Gene expression analysis
 - scRNA-seq processing and population-specific signatures
 - CyTOF sample acquisition, staining and data processing
 - Multiplex immunofluorescence
 - Tertiary lymphoid structure and lymphoid aggregate calling from H&E
 - Comprehensive genomic profiling (CGP) by FoundationOne
- **QUANTIFICATION AND STATISTICAL ANALYSIS**
 - Survival and statistical analysis

SUPPLEMENTAL INFORMATION

Supplemental information can be found online at <https://doi.org/10.1016/j.ccell.2022.02.002>.

ACKNOWLEDGMENTS

We thank all the patients who kindly provided tumor samples for this study. Finally, the authors thank all of the investigators and staff involved in the OAK and POPLAR studies. Editorial support for this manuscript was provided by Anshin Biosolutions. Multiplex immunofluorescence was performed by Ultivue. The graphical abstract was produced using Servier Medical Art (<https://smart.servier.com>), licensed under CC BY 3.0. This work was funded by Genentech/Roche.

AUTHOR CONTRIBUTIONS

N.S.P. and D.S.S. conceived the project. N.S.P., B.Y.N., S.M., H.K., W.Z., P.E.d.A., J.H.C., and A.C.E. performed experiments. N.S.P., B.Y.N., S.M., S.S., H.K., W.Z., A.A.-Y., C.T., W.E.O., and R.B. analyzed data. N.S.P., B.Y.N., S.M., H.K., W.Z., C.T., J.L.G., L.R., S.J., M.P., A.W.H., W.E.O., M.B., J.G., and R.B. guided data analysis. N.S.P., B.Y.N., S.M., S.S., and R.B. wrote the manuscript with input from all authors. All authors contributed to data interpretation and discussion of results and commented on the manuscript.

DECLARATION OF INTERESTS

All authors are employees and stockholders of Genentech/Roche. N.S.P., B.Y.N., S.M., and R.B. are co-inventors on a provisional patent application filed by Genentech/Roche relating to this manuscript.

Received: January 26, 2021
Revised: November 11, 2021
Accepted: February 2, 2022
Published: February 24, 2022

SUPPORTING CITATIONS

The following reference appears in the supplemental information: Liberzon et al. (2015).

REFERENCES

Adler, L.N., Jiang, W., Bhamidipati, K., Millican, M., Macaubas, C., Hung, S.-C., and Mellins, E.D. (2017). The other function: class II-restricted antigen presentation by B cells. *Front. Immunol.* **8**, 319.
Aiba, Y., Yamazaki, T., Okada, T., Gotoh, K., Sanjo, H., Ogata, M., and Kurosaki, T. (2006). BANK negatively regulates Akt activation and subsequent B cell responses. *Immunity* **24**, 259–268.

Al-Shibli, K.I., Donnem, T., Al-Saad, S., Persson, M., Bremnes, R.M., and Busund, L.-T. (2008). Prognostic effect of epithelial and stromal lymphocyte infiltration in non-small cell lung cancer. *Clin. Cancer Res.* **14**, 5220–5227.

Banchereau, R., Chitre, A.S., Scherl, A., Wu, T.D., Patil, N.S., Almeida, P.D., Kadel, E.E., III, Madireddi, S., Au-Yeung, A., Takahashi, C., et al. (2021a). Intratumoral CD103+ CD8+ T cells predict response to PD-L1 blockade. *J. Immunother. Cancer* **9**, e002231.

Banchereau, R., Leng, N., Zill, O., Sokol, E., Liu, G., Pavlick, D., Maund, S., Liu, L.-F., Kadel, E., Baldwin, N., et al. (2021b). Molecular determinants of response to PD-L1 blockade across tumor types. *Nat. Commun.* **12**, 3969.

Blenman, K.R.M., He, T.-F., Frankel, P.H., Ruel, N.H., Schwartz, E.J., Krag, D.N., Tan, L.K., Yim, J.H., Mortimer, J.E., Yuan, Y., et al. (2018). Sentinel lymph node B cells can predict disease-free survival in breast cancer patients. *npj Breast Cancer* **4**, 28.

Bruno, T.C., Ebner, P.J., Moore, B.L., Squalls, O.G., Waugh, K.A., Eruslanov, E.B., Singhal, S., Mitchell, J.D., Franklin, W.A., Merrick, D.T., et al. (2017). Antigen-presenting intratumoral B cells affect CD4+ TIL phenotypes in non-small cell lung cancer patients. *Cancer Immunol. Res.* **5**, 898–907.

Butler, A., Hoffman, P., Smibert, P., Papalexi, E., and Satija, R. (2018). Integrating single-cell transcriptomic data across different conditions, technologies, and species. *Nat. Biotechnol.* **36**, 411–420.

Cabrita, R., Lauss, M., Sanna, A., Donia, M., Larsen, M.S., Mitra, S., Johansson, I., Phung, B., Harbst, K., Vallon-Christersson, J., et al. (2020). Tertiary lymphoid structures improve immunotherapy and survival in melanoma. *Nature* **577**, 561–565.

Camidge, D.R., Doebele, R.C., and Kerr, K.M. (2019). Comparing and contrasting predictive biomarkers for immunotherapy and targeted therapy of NSCLC. *Nat. Rev. Clin. Oncol.* **16**, 341–355.

Dieu-Nosjean, M.-C., Goc, J., Giraldo, N.A., Sautès-Fridman, C., and Fridman, W.H. (2014). Tertiary lymphoid structures in cancer and beyond. *Trends Immunol.* **35**, 571–580.

Duma, N., Santana-Davila, R., and Molina, J.R. (2019). Non-small cell lung cancer: epidemiology, screening, diagnosis, and treatment. *Mayo Clin. Proc.* **94**, 1623–1640.

Eisenhauer, E.A., Therasse, P., Bogaerts, J., Schwartz, L.H., Sargent, D., Ford, R., Dancey, J., Arbuck, S., Gwyther, S., Mooney, M., et al. (2009). New response evaluation criteria in solid tumours: revised RECIST guideline (version 1.1). *Eur. J. Cancer* **45**, 228–247.

Facchinetti, F., Bordi, P., Leonetti, A., Buti, S., and Tiseo, M. (2018). Profile of atezolizumab in the treatment of metastatic non-small-cell lung cancer: patient selection and perspectives. *Drug Des. Dev. Ther.* **12**, 2857–2873.

Fehrenbacher, L., Spira, A., Ballinger, M., Kowanetz, M., Vansteenkiste, J., Mazieres, J., Park, K., Smith, D., Artal-Cortes, A., Lewanski, C., et al. (2016). Atezolizumab versus docetaxel for patients with previously treated non-small-cell lung cancer (POPLAR): a multicentre, open-label, phase 2 randomised controlled trial. *Lancet* **387**, 1837–1846.

Fujimoto, M., Yoshizawa, A., Sumiyoshi, S., Sonobe, M., Kobayashi, M., Koyanagi, I., Aini, W., Tsuruyama, T., Date, H., and Haga, H. (2013). Stromal plasma cells expressing immunoglobulin G4 subclass in non-small cell lung cancer. *Hum. Pathol.* **44**, 1569–1576.

Gandara, D.R., Paul, S.M., Kowanetz, M., Schleifman, E., Zou, W., Li, Y., Rittmeyer, A., Fehrenbacher, L., Otto, G., Malboeuf, C., et al. (2018). Blood-based tumor mutational burden as a predictor of clinical benefit in non-small-cell lung cancer patients treated with atezolizumab. *Nat. Med.* **24**, 1441–1448.

Gentles, A.J., Newman, A.M., Liu, C.L., Bratman, S.V., Feng, W., Kim, D., Nair, V.S., Xu, Y., Khuong, A., Hoang, C.D., et al. (2015). The prognostic landscape of genes and infiltrating immune cells across human cancers. *Nat. Med.* **21**, 938–945.

Germain, C., Gnjatich, S., Tamzalit, F., Knockaert, S., Remark, R., Goc, J., Lepelle, A., Becht, E., Katsahian, S., Bizouard, G., et al. (2014). Presence of B cells in tertiary lymphoid structures is associated with a protective immunity in patients with lung cancer. *Am. J. Respir. Crit. Care* **189**, 832–844.

- Grant, M.J., Herbst, R.S., and Goldberg, S.B. (2021). Selecting the optimal immunotherapy regimen in driver-negative metastatic NSCLC. *Nat. Rev. Clin. Oncol.* **18**, 625–644.
- Greiff, V., Bhat, P., Cook, S.C., Menzel, U., Kang, W., and Reddy, S.T. (2015). A bioinformatic framework for immune repertoire diversity profiling enables detection of immunological status. *Genome Med.* **7**, 49.
- Helmink, B.A., Reddy, S.M., Gao, J., Zhang, S., Basar, R., Thakur, R., Yizhak, K., Sade-Feldman, M., Blando, J., Han, G., et al. (2020). B cells and tertiary lymphoid structures promote immunotherapy response. *Nature* **577**, 549–555.
- Herbst, R.S., Giaccone, G., Marinis, F.D., Reinmuth, N., Vergnenegre, A., Barrios, C.H., Morise, M., Felip, E., Andric, Z., Geater, S., et al. (2020). Atezolizumab for first-line treatment of PD-L1–selected patients with NSCLC. *N. Engl. J. Med.* **383**, 1328–1339.
- Kim, N., Kim, H.K., Lee, K., Hong, Y., Cho, J.H., Choi, J.W., Lee, J.-I., Suh, Y.-L., Ku, B.M., Eum, H.H., et al. (2020). Single-cell RNA sequencing demonstrates the molecular and cellular reprogramming of metastatic lung adenocarcinoma. *Nat. Commun.* **11**, 2285.
- Knief, J., Reddemann, K., Petrova, E., Herhahn, T., Wellner, U., and Thorns, C. (2016). High density of tumor-infiltrating B-lymphocytes and plasma cells signifies prolonged overall survival in adenocarcinoma of the esophagogastric junction. *Anticancer Res.* **36**, 5339–5346.
- Lambrechts, D., Wauters, E., Boeckx, B., Aibar, S., Nittner, D., Burton, O., Bassez, A., Decaluwé, H., Pircher, A., Eynde, K.V.D., et al. (2018). Phenotype molding of stromal cells in the lung tumor microenvironment. *Nat. Med.* **24**, 1277–1289.
- Lawrence, M., Huber, W., Pagès, H., Aboyoun, P., Carlson, M., Gentleman, R., Morgan, M.T., and Carey, V.J. (2013). Software for computing and annotating genomic ranges. *PLoS Comput. Biol.* **9**, e1003118.
- Liberzon, A., Birger, C., Thorvaldsdóttir, H., Ghandi, M., Mesirov, J.P., and Tamayo, P. (2015). The molecular signatures database hallmark gene set collection. *Cell Syst.* **1**, 417–425.
- Lisberg, A., Cummings, A., Goldman, J.W., Bornazyan, K., Reese, N., Wang, T., Coluzzi, P., Ledezma, B., Mendenhall, M., Hunt, J., et al. (2018). A phase II study of pembrolizumab in EGFR-mutant, PD-1+, tyrosine kinase inhibitor naïve patients with advanced NSCLC. *J. Thorac. Oncol.* **13**, 1138–1145.
- Lohr, M., Edlund, K., Botling, J., Hammad, S., Hellwig, B., Othman, A., Berglund, A., Lambe, M., Holmberg, L., Ekman, S., et al. (2013). The prognostic relevance of tumour-infiltrating plasma cells and immunoglobulin kappa C indicates an important role of the humoral immune response in non-small cell lung cancer. *Cancer Lett.* **333**, 222–228.
- Mariathasan, S., Turley, S.J., Nickles, D., Castiglioni, A., Yuen, K., Wang, Y., Kadel, E.E., III, Koepfen, H., Astarita, J.L., Cubas, R., et al. (2018). TGF β attenuates tumour response to PD-L1 blockade by contributing to exclusion of T cells. *Nature* **554**, 544–548.
- Maynard, A., McCoach, C.E., Rotow, J.K., Harris, L., Haderk, F., Kerr, D.L., Yu, E.A., Schenk, E.L., Tan, W., Zee, A., et al. (2020). Therapy-induced evolution of human lung cancer revealed by single-cell RNA sequencing. *Cell* **182**, 1232–1251.e22.
- Mok, T.S.K., Wu, Y.-L., Kudaba, I., Kowalski, D.M., Cho, B.C., Tuma, H.Z., Castro, G., Srimuninnimit, V., Laktionov, K.K., Bondarenko, I., et al. (2019). Pembrolizumab versus chemotherapy for previously untreated, PD-L1-expressing, locally advanced or metastatic non-small-cell lung cancer (KEYNOTE-042): a randomised, open-label, controlled, phase 3 trial. *Lancet* **393**, 1819–1830.
- Nelson, B.H. (2010). CD20 + B cells: the other tumor-infiltrating lymphocytes. *J. Immunol.* **185**, 4977–4982.
- Patel, A.J., Richter, A., Drayson, M.T., and Middleton, G.W. (2020). The role of B lymphocytes in the immuno-biology of non-small-cell lung cancer. *Cancer Immunol. Immunother.* **69**, 325–342.
- Petitprez, F., Reyniès, A.D., Keung, E.Z., Chen, T.W.-W., Sun, C.-M., Calderaro, J., Jeng, Y.-M., Hsiao, L.-P., Lacroix, L., Bougouin, A., et al. (2020). B cells are associated with survival and immunotherapy response in sarcoma. *Nature* **577**, 556–560.
- Reck, M., Mok, T.S.K., Nishio, M., Jotte, R.M., Cappuzzo, F., Orlandi, F., Stroyakovskiy, D., Nogami, N., Rodríguez-Abreu, D., Moro-Sibilot, D., et al. (2019). Atezolizumab plus bevacizumab and chemotherapy in non-small-cell lung cancer (IMpower150): key subgroup analyses of patients with EGFR mutations or baseline liver metastases in a randomised, open-label phase 3 trial. *Lancet Respir. Med.* **7**, 387–401.
- Ritchie, M.E., Phipson, B., Wu, D., Hu, Y., Law, C.W., Shi, W., and Smyth, G.K. (2015). Limma powers differential expression analyses for RNA-sequencing and microarray studies. *Nucleic Acids Res.* **43**, e47.
- Rittmeyer, A., Barlesi, F., Waterkamp, D., Park, K., Ciardiello, F., Pawel, J.V., Gadgeel, S.M., Hida, T., Kowalski, D.M., Dols, M.C., et al. (2017). Atezolizumab versus docetaxel in patients with previously treated non-small-cell lung cancer (OAK): a phase 3, open-label, multicentre randomised controlled trial. *Lancet* **389**, 255–265.
- Ruffin, A.T., Cillo, A.R., Tabib, T., Liu, A., Onkar, S., Kunning, S.R., Lampenfeld, C., Atiya, H.I., Abecassis, I., Kürten, C.H.L., et al. (2021). B cell signatures and tertiary lymphoid structures contribute to outcome in head and neck squamous cell carcinoma. *Nat. Commun.* **12**, 3349.
- Shaffer, A.L., Shapiro-Shelef, M., Iwakoshi, N.N., Lee, A.-H., Qian, S.-B., Zhao, H., Yu, X., Yang, L., Tan, B.K., Rosenwald, A., et al. (2004). XBP1, downstream of Blimp-1, expands the secretory apparatus and other organelles, and increases protein synthesis in plasma cell differentiation. *Immunity* **21**, 81–93.
- Sharonov, G.V., Serebrovskaya, E.O., Yuzhakova, D.V., Britanova, O.V., and Chudakov, D.M. (2020). B cells, plasma cells and antibody repertoires in the tumour microenvironment. *Nat. Rev. Immunol.* **20**, 294–307.
- Skoulidis, F., Goldberg, M.E., Greenawald, D.M., Hellmann, M.D., Awad, M.M., Gainor, J.F., Schrock, A.B., Hartmaier, R.J., Trabucco, S.E., Gay, L., et al. (2018). STK11/LKB1 mutations and PD-1 inhibitor resistance in KRAS-mutant lung adenocarcinoma. *Cancer Discov.* **8**, 822–835.
- Socinski, M.A., Jotte, R.M., Cappuzzo, F., Orlandi, F., Stroyakovskiy, D., Nogami, N., Rodríguez-Abreu, D., Moro-Sibilot, D., Thomas, C.A., Barlesi, F., et al. (2018). Atezolizumab for first-line treatment of metastatic nonsquamous NSCLC. *N. Engl. J. Med.* **378**, 2288–2301.
- Vasaturo, A., and Galon, J. (2019). Multiplexed immunohistochemistry for immune cell phenotyping, quantification and spatial distribution in situ. *Methods Enzymol.* **635**, 51–66.
- Waldman, A.D., Fritz, J.M., and Lenardo, M.J. (2020). A guide to cancer immunotherapy: from T cell basic science to clinical practice. *Nat. Rev. Immunol.* **20**, 651–668.
- Wohlhieter, C.A., Richards, A.L., Uddin, F., Hulton, C.H., Quintanal-Villalonga, À., Martin, A., Stanchina, E.D., Bhanot, U., Asher, M., Shah, N.S., et al. (2020). Concurrent mutations in STK11 and KEAP1 promote ferroptosis protection and SCD1 dependence in lung cancer. *Cell Rep.* **33**, 108444.
- Wouters, M.C.A., and Nelson, B.H. (2018). Prognostic significance of tumor-infiltrating B cells and plasma cells in human cancer. *Clin. Cancer Res.* **24**, 6125–6135.
- Zhao, Y., Lee, C.K., Lin, C.-H., Gassen, R.B., Xu, X., Huang, Z., Xiao, C., Bonorino, C., Lu, L.-F., Bui, J.D., et al. (2019). PD-L1:CD80 cis-heterodimer triggers the co-stimulatory receptor CD28 while repressing the inhibitory PD-1 and CTLA-4 pathways. *Immunity* **51**, 1059–1073.e9.

STAR★METHODS

KEY RESOURCES TABLE

REAGENT or RESOURCE	SOURCE	IDENTIFIER
Antibodies		
Anti-human CD3, clone BC33	Biocare Medical	Cat#ACI3170CF
Anti-human CD8, clone C8/144B	Biocare Medical	Cat#ACI3160CF
Anti-human CD20, clone L26	ThermoFisher	Cat#14-0202-82
Anti-human CD138, clone EPR6454	Abcam	Cat#Ab226108
Anti-human CD68, clone KP1	Biocare Medical	Cat#CM033CF
Anti-human CD163, clone EPR19518	Abcam	Cat#ab213612
Anti-human PanCK, clone AE1/AE3	Bethyl Laboratories	Cat#A500-019A
Biological samples		
OAK NSCLC samples (n=699)	This study	N/A
POPLAR NSCLC samples (n=192)	This study	N/A
Human NSCLC tissue collection (n=23)	Avaden Biosciences	N/A
Human NSCLC tissue collection for CyTOF (n=6)	Discovery Life Sciences	N/A
Critical commercial assays		
Illumina TruSeq RNA Library Prep for Enrichment	Illumina	Cat#20020189
Illumina TruSeq RNA Enrichment	Illumina	Cat#20020490
Illumina TruSeq RNA Exome Panel	Illumina	Cat#20020183
Targeted Gene Alterations	Foundation Medicine	FoundationOne (T7)
Deposited data		
Raw and processed RNA-seq data from OAK (n=699) and POPLAR (n=192).	European Genome-phenome Archive	EGA: EGAS00001005013
Relevant clinical data from OAK and POPLAR.	European Genome-phenome Archive	EGA: EGAS00001005013
OAK 22C3 PD-L1 TC status (n=361), relevant mutation status (n=517), and tTMB status (n=425).	European Genome-phenome Archive	EGA: EGAS00001005013
NSCLC scRNA-seq	Kim et al., 2020	GSE131907
NSCLC scRNA-seq	Maynard et al., 2020	https://drive.google.com/drive/folders/1qZJiFFf9ggfi0Sn79n8uOhWqVdfvjKHp
NSCLC scRNA-seq	Lambrechts et al., 2018	https://gbiomed.kuleuven.be/english/research/50000622/laboratories/54213024/scRNAseq-NSCLC
NSCLC CyTOF	Banchereau et al., 2021a	https://flowrepository.org/id/FR-FCM-Z3NA
Software and algorithms		
R Statistical Software version 4.0.0	The R Foundation	https://www.r-project.org/
survminer package version 0.4.3	CRAN Repository	https://cran.r-project.org/web/packages/survminer/index.html
survival package version 2.42-3	CRAN Repository	https://cran.r-project.org/web/packages/survival/index.html
qusage package v2.18.0	Bioconductor	https://www.bioconductor.org/packages/release/bioc/html/qusage.html
limma package v3.50.0	Bioconductor	https://bioconductor.org/packages/release/bioc/html/limma.html

RESOURCE AVAILABILITY

Lead contact

Further information and requests should be directed and will be fulfilled by the lead contact, Namrata Patil (patil.namrata@gene.com)

Materials availability

This study did not generate new unique reagents.

Data and code availability

Raw and processed transcriptomic data, relevant mutation status, and limited clinical data has been deposited at the European Genome-phenome Archive (EGA), which is hosted by the EBI and the CRG, under accession number EGA: EGAS00001005013. Additional clinical data is available via request from vivli.org.

EXPERIMENTAL MODEL AND SUBJECT DETAILS

Patient population and biomarker collection

This study was performed using tissue samples from the open-label, randomized Phase 2 POPLAR (NCT01903993) and Phase 3 OAK trials (NCT02008227), which evaluated atezolizumab versus docetaxel in patients with NSCLC who progressed following platinum-based chemotherapy (Fehrenbacher et al., 2016; Rittmeyer et al., 2017), and enrolled 287 and 1225 patients, respectively. Patients in all trials received either 1200 mg atezolizumab IV every 3 weeks (q3w) until disease progression or loss of clinical benefit, or 75 mg/m² docetaxel IV q3w until PD. POPLAR and OAK studies demonstrated significant improvement in OS with atezolizumab vs. docetaxel, regardless of PD-L1 expression (Fehrenbacher et al., 2016; Rittmeyer et al., 2017). No crossover was allowed, and OS was the primary endpoint. Both the POPLAR and OAK studies were performed in full accordance with the guidelines for Good Clinical Practice and the Declaration of Helsinki, and all patients gave written informed consent. Protocol approval was obtained from independent ethics committees for each participating site for both studies and an independent data monitoring committee reviewed the safety data (Fehrenbacher et al., 2016; Rittmeyer et al., 2017) (Table S5). Pre-treatment tissue was collected from paraffin-embedded tissue (FFPE) from 699 patients from OAK and 192 patients from POPLAR. FFPE tumor tissue was stained for PD-L1 by IHC using a proprietary diagnostic anti-human PD-L1 monoclonal antibody (22C3).

METHOD DETAILS

Gene expression analysis

RNA extraction was conducted for all samples that contained a minimum of 20% TC, greater than 75% of the tumors had more than 45% tumor purity. H&E images were marked for macro-dissection by a pathologist. RNA (High Pure FFPE RNA Isolation Kit, Roche) was extracted from the macro-dissected sections. All transcriptome profiles were generated using TruSeq RNA Access technology (Illumina®) for 192 patients from the POPLAR and 699 patients from OAK. Alignment of RNAseq reads to ribosomal RNA sequences was performed to remove ribosomal reads. NCI Build 38 human reference genome was then used to align the remaining reads using GSNAP version 2013-10-10 wherein a maximum of two mismatches per 75 base sequence (parameters: '-M 2 -n 10 -B 2 -i 1 -N 1 -w 200000 -E 1 -pairmax-rna=200000 -clip-overlap) was allowed. Transcript annotation was based on the Ensembl genes database (release 77). To quantify gene expression levels, the number of reads mapped to the exons of each RefSeq gene was calculated in a strand-specific manner using the functionality provided by the R package *Genomic Alignments* (Bioconductor) (Lawrence et al., 2013; Mariathasan et al., 2018).

To identify biology associated with OS benefit with atezolizumab, we grouped patients with either survival of <6 months or >12 months (Fehrenbacher et al., 2016). Differentially expressed genes between these two groups were determined using the R package *limma* (Bioconductor), which implements an empirical Bayesian approach to estimate gene expression changes using moderated t-tests (Ritchie et al., 2015). All expression based associations with outcomes were first tested in OAK and then validated in POPLAR.

scRNA-seq processing and population-specific signatures

Samples were obtained from Gene Expression Omnibus (GEO) under accession GSE131907 as raw UMI counts per cell. Additionally, annotations of cell type and sample origin for each cell were retrieved. These cell type annotations from the authors were used to isolate B cells from tumor and normal adjacent tissue as well as draining lymph nodes from the expression matrix. The Seurat package (v3.1.4) (Butler et al., 2018) was used for downstream analysis of B cells in R (3.6.2).

We filtered cells with less than 500 measured genes or more than 10 percent mitochondrial reads and normalized the expression counts of the remaining cells to log(CPM/100+1). Principal component analysis was performed on the 2000 most variable genes, and the first 30 principal components were used for UMAP dimensionality reduction and graph-based clustering.

Clusters were determined using a resolution of 0.3. Markers for each cluster were detected by comparing all cells in a particular cluster to the rest of the cells in the dataset using Wilcoxon's rank sum test adjusted for multiple testing with Benjamini Hochberg. From the initial dataset we removed non-B cell contaminant clusters (*CD3*⁺ T cells, *GZMB*⁺ *LILRA4*⁺ pDCs, and *HBA2*⁺ red blood

cells). After removal of these contaminant cells, we re-ran variable gene detection, PCA, and UMAP dimensionality reduction with the parameters described above, but using a resolution of 0.05. Markers for each B cell subset were identified as genes with an adjusted p -value <0.001 and $\log_{2}FC >0.5$ comparing B cells in a cluster to all other cells in the dataset. To guarantee B-cell specific expression of markers, we further only retained marker genes that were not expressed by non-B cells in the full dataset including stromal, tumor, and non-B immune cells (retained genes: average $\log(CPM/100+1) <1$ across non B cell populations). To increase sensitivity further, we removed additional genes with even low expression found in tumor/epithelial cells (given these cells represent the majority of cells in most samples; retained genes: average CPM in epithelial cells <0.08). Heatmaps for visual comparisons were created using the `heatmap` R package (1.0.12).

The dataset from Maynard et al. was retrieved as a Seurat object provided by the authors (<https://drive.google.com/drive/folders/1qZJiFFf9ggfi0Sn79n8uOhWqVDfvjKHp>). Data was normalized to $\log(CPM/10+1)$ and dimensionality reduction and clustering was performed as described above, here using 30 PCs and a resolution of 0.5. We focused our analysis on B cells (identified based on *CD79A* expression in all clusters) and performed dimensionality reduction and clustering on this subset of cells (PCs: 30; resolution 0.1). To assign a score to each cell for the three gene signatures obtained in the dataset from Kim et al., we used the `addModuleScore` function in Seurat.

B cell expression data from Lambrechts et al. were directly obtained from SCoPe (<https://gbiomed.kuleuven.be/english/research/50000622/laboratories/54213024/scRNAseq-NSCLC>) in loom format. Data was converted into a Seurat object (`as.Seurat` function) and normalized to $\log(CPM/100+1)$. We used 30 PCs and a resolution of 0.01 for dimensionality reduction and clustering. Scores for gene signatures in cells were assigned as described above.

CyTOF sample acquisition, staining and data processing

Six fresh NSCLC tumor samples were procured from a commercial vendor (Discovery Life Sciences) as part of adult patients undergoing surgical resection, as described (Banchereau et al., 2021a). We complied with all ethical standards of the Roche Ethics Committee. Informed consent was obtained from all sampled individuals. After overnight fixation, cells were washed with 3 mL of MaxPar® cell staining buffer and centrifuged at $800 \times g$ for 5 minutes. After aspiration of the wash buffer and resuspension of the cell pellet, another round of wash was performed with 4 mL of MaxPar® Water (Fluidigm). Cells were resuspended in 1 mL of MaxPar® Water and counted. After obtaining cell counts, 3 mL of MaxPar® Water was added and cells were pelleted one final time prior to instrument acquisition. Before introduction into the Helios™, a CyTOF® System (Fluidigm), pelleted cells were resuspended with 1X MaxPar® Water containing EQ™ Four Element Calibration Beads (Fluidigm) then filtered using a 12 x 75 mm tube with a 35 μ m nylon mesh cell-strainer cap (Corning). All FCS files were normalized together using the MATLAB® (MathWorks) normalizer and analyzed using FlowJo® software (FlowJo, LLC, Ashland, Oregon). Protein marker expression intensities from mass cytometry analysis were aggregated from multiple samples and transformed using the inverse hyperbolic sine function. Dimensionality reduction was applied to the transformed expression matrix using the uniform manifold approximation and projection (UMAP) package with the following default parameters: `min_dist: 0.1`, `n_neighbors: 15`, `n_components: 2`, and `metric: euclidean`. Individual samples were downsampled to 8,000 cells per sample in CD45⁺ and CD8⁺ populations. UMAP coordinates were appended to “.fcs” files as additional channels for integration with manual gating analysis in FlowJo (FlowJo, LLC).

Multiplex immunofluorescence

Triple immunofluorescence (CD8/CD79/Ki-67) was performed on 4 μ m sections of formalin fixed paraffin embedded (FFPE) tumor samples from our clinical studies, following deparaffinization, rehydration, and epitope retrieval with Target Retrieval Solution pH 6 for 20 minutes at 99°C. Each staining round began with quenching in 3% hydrogen peroxide. Sections were incubated in anti-CD79a rabbit monoclonal (SP18) (Thermo Fischer Scientific, MA5-14556) diluted 1:300, detected with PowerVision Poly-horseradish peroxidase (HRP) anti-rabbit, and amplified with Alexa-Fluor 488 Tyramide. Elution was performed in Target Retrieval Solution pre-warmed to 99°C for 20 minutes. Sections were incubated in anti-CD8 mouse monoclonal C8/144B (Dako, M7103) diluted to 1.5 μ g/ml, detected with PowerVision Poly-HRP anti-mouse, and amplified with Alexa-Fluor 647 Tyramide. Following an elution step, sections were incubated in anti-Ki67 mouse monoclonal (MIB-1) (Dako, M7240) diluted to 1 μ g/ml, detected with PowerVision Poly-HRP anti-mouse, and amplified with Alexa-Fluor 555 Tyramide. Slides were counterstained with 4',6-diamidino-2-phenylindole (DAPI). Images of fluorescent slides were acquired on a NanoZoomer XR.

An NSCLC tissue collection ($n = 23$) was procured from Avaden Biosciences for orthogonal validation of TLS/LA calling and bulk RNA-seq deconvolution. Procured samples had appropriate Institutional Review Board (IRB) approval. The mIF panel was designed to capture plasma cells (pan-cytokeratin [panCK], CD3, CD8, CD163/68 cocktail, CD20, CD138, BCMA, DC-LAMP). Multiplex IF staining was performed as previously described (Vasaturo and Galon, 2019). In brief, FFPE samples are dewaxed and epitope retrieval is performed. After blocking, the slides are incubated with DNA-barcoded primary antibodies. All the targets are amplified and then mixed with fluorescently-tagged probes for hybridization and labeling. Images are then serially acquired for each channel and thresholds are set for each channel to assign positivity. These data are then used to quantify cellular phenotypes of interest. In a blinded review, a trained pathologist confirmed that the non-tumor CD138+/panCK- cells exhibited classic plasma cell cytological features. For comparison to RNA-seq data, the mIF defined cellular phenotypes were normalized to the number of panCK⁺ cells to account for differences in tumor/slide size between samples. To compare correlation of mIF plasma cells with other mIF identified cell phenotypes and leave-one-out cross-validation approach.

Tertiary lymphoid structure and lymphoid aggregate calling from H&E

TLS were identified on H&E stained FFPE sections by a board-certified hemato-pathologist (HK); definition of a TLS required presence of a true germinal center with cellular heterogeneity (centrocytes, centroblasts, tingible-body macrophages) surrounded by a zone of small lymphoid cells and - in most cases - focal accumulations of plasma cells. Lymphoid aggregates (LA) on the other hand were defined as well-circumscribed, rather dense aggregates of mostly small lymphoid cells without the cellular diversity seen in TLS (Dieu-Nosjean et al., 2014).

Comprehensive genomic profiling (CGP) by FoundationOne

Comprehensive genomic profiling was carried out as previously described (Banchereau et al., 2021b). In brief, hybrid capture was performed on FFPE tumor DNA libraries and sequenced to high uniform depth (>500X). We only considered mutations in genes previously identified to impact CPI outcomes (EGFR, STK11, KEAP1). tTMB was calculated as previously described (Gandara et al., 2018).

QUANTIFICATION AND STATISTICAL ANALYSIS

Survival and statistical analysis

The Wilcoxon and Chi-squared tests were used where indicated. For survival analyses, the log-rank test was used to compare Kaplan-Meier survival curves. Cox proportional hazards regression models were used to generate hazard ratios and 95% confidence intervals as stratified by distribution-based cut-points (e.g. tertiles), as described in the corresponding legend and text. Multivariable Cox proportional hazards regression models were used to compare the interdependence of distinct biomarkers for prediction of OS benefit. Differential gene expression analyses were conducted using the limma R package. All *P*-values are FDR corrected unless otherwise indicated. All analyses were conducted using R v.4.0.0 with the survminer, survival, and limma packages.